© 2017. Published by The Company of Biologists Ltd | Journal of Cell Science (2017) 130, 1217-1223 doi:10.1242/jcs.199042

SHORT REPORT

Microtubule-associated protein-4 controls nanovesicle dynamics and T cell activation

Eugenio Bustos-Morán[1,2], Noelia Blas-Rus[1,2], Noa Beatriz Martin-Cófreces[1,2,3] and Francisco Sánchez-Madrid[1,2,3,*]

ABSTRACT

The immune synapse (IS) is a specialized structure formed at the contact area between T lymphocytes and antigen-presenting cells (APCs) that is essential for the adaptive immune response. Proper T cell activation requires its polarization towards the APC, which is highly dependent on the tubulin cytoskeleton. Microtubule-associated protein-4 (MAP4) is a microtubule (MT)-stabilizing protein that controls MTs in physiological processes, such as cell division, migration, vesicular transport or primary cilia formation. In this study, we assessed the role of MAP4 in T cell activation. MAP4 decorates the pericentrosomal area and MTs of the T cell, and it is involved in MT detyrosination and stable assembly in response to T cell activation. In addition, MAP4 prompts the timely translocation of the MT-organizing center (MTOC) towards the IS and the dynamics of signaling nanovesicles that sustains T cell activation. However, MAP4 acts as a negative regulator of other T cell activation-related signals, including diacylglycerol (DAG) production and IL2 secretion. Our data indicate that MAP4 acts as a checkpoint molecule that balances positive and negative hallmarks of T cell activation.

KEY WORDS: MAP4, T cell activation, Vesicle dynamics, Microtubules

INTRODUCTION

The recognition of an antigen peptide on the surface of an antigen-presenting cell (APC) triggers a signaling cascade leading to the formation of a polarized and specialized structure called the immune synapse (IS) (Huppa and Davis, 2003). Its proper formation is tightly regulated by the interplay of the actin and tubulin cytoskeletons (Soares et al., 2013). The microtubule (MT) network is polarized at the IS due to the translocation of the MT-organizing center (MTOC) towards the contact area, leading to the rearrangement of the tubulin cytoskeleton by polymerization of new MTs (Martín-Cófreces et al., 2014).

MT-associated proteins (MAPs) are proteins that bind to MTs and regulate their dynamics, growth, catastrophe and association to other molecular complexes. MAP4 is the most abundant MAP in non-neuronal tissues. *In vitro*, MAP4 promotes MT assembly and stabilization (Nguyen et al., 1999, 1998). Moreover, it is involved in some physiological processes such as cilia formation (Ghossoub et al., 2013) and myotube organization (Mogessie et al., 2015). Most studies regarding MAP4 have addressed its role in a cell division context, controlling the assembly of the mitotic spindle and the orientation of the centrosome (Chang et al., 2001; Samora et al., 2011). In this work, we assessed the role of MAP4 in T cell activation and polarization. We have identified a new role of MAP4 in CD3ζ (also known as CD247)-bearing nanovesicle dynamics at the IS and T cell activation.

RESULTS AND DISCUSSION

MAP4 regulates MT stabilization and MTOC translocation at the IS

In order to assess MAP4 location in CD4+ T cells during IS formation, MAP4 was immunostained in Jurkat T cells conjugated with staphylococcal enterotoxin E (SEE)-pulsed Raji B cells (SEE-APCs) (Fig. 1A). The MAP4 staining pattern was similar to that of α-tubulin, decorating the MTOC. MAP4 dynamics was assessed upon T-cell–APC contact formation in Jurkat T cells co-transfected with rodent MAP4 coupled to GFP and α-tubulin–mCherry and conjugated with SEE-APCs. Time-lapse confocal microscopy revealed a similar behavior for both proteins (Fig. S1; Movie 1).

In most systems, MAP4 appears to be mainly colocalized with MTs (Chang et al., 2001; Cheng et al., 2010; Samora et al., 2011). Moreover, in T cells, most MAP4 appeared to be concentrated around the MTOC. These results suggest that, in T cells, MAP4 may be important for the assembly of new MTs during IS formation. To address this, we first measured the ability of MTs to reassemble in control cells or cells depleted of MAP4 using specific siRNAs (denoted MAP4 knockdown; MAP4KD) (Fig. 1B). T cells were treated with nocodazole (8 µM) to fully depolymerize MTs, and their re-assembly assessed upon washout of the inhibitor. Most MAP4KD cells displayed depolymerized tubulin, which concentrated around the nucleus (Fig. 1C), indicating that MAP4 is required for the reassembly of MTs. To assess whether MAP4 participates in MT stabilization in response to TCR signals, we studied the de-tyrosination (Glu) of α-tubulin, a MT stability marker observed upon TCR activation, in T cells. Interestingly, the increase of de-tyrosinated tubulin upon TCR triggering was prevented in MAP4KD cells (Fig. 1D). However, no changes in the overall efficiency of conjugate formation were detected (Fig. 1E). Taken together, these results indicate that MAP4 is an important mediator of MT assembly, likely by controlling MT stability, in response to signals emanating from the IS.

MTOC reorientation is a hallmark of T cell activation during the formation of the IS that may depend on MT dynamics (Martín-Cófreces et al., 2014). Consequently, we next analyzed the distance of the MTOC to the IS at different time points of conjugation in control and in MAP4KD Jurkat T cells. A significant increase in this parameter was observed in MAP4KD cells compared to control cells shortly after activation, which disappeared after longer times (Fig. 1F). Reconstitution of MAP4 KD cells with GFP-MAP4 construction rescued MTOC translocation (Fig. 1G). These results indicate that MAP4 controls the timely translocation of the MTOC to the IS.

[1]Laboratory of Intercellular communication, Fundación CNIC, Madrid 28029, Spain. [2]Servicio de Inmunología, Hospital Universitario de la Princesa, UAM, IIS-IP, Madrid 28006, Spain. [3]CIBER Cardiovascular, ISCIII, Madrid, 28029, Spain.

*Author for correspondence (fsmadrid@salud.madrid.org)

Received 27 October 2016; Accepted 7 February 2017

Journal of Cell Science (2017) 130, 1217-1223 doi:10.1242/jcs.199042

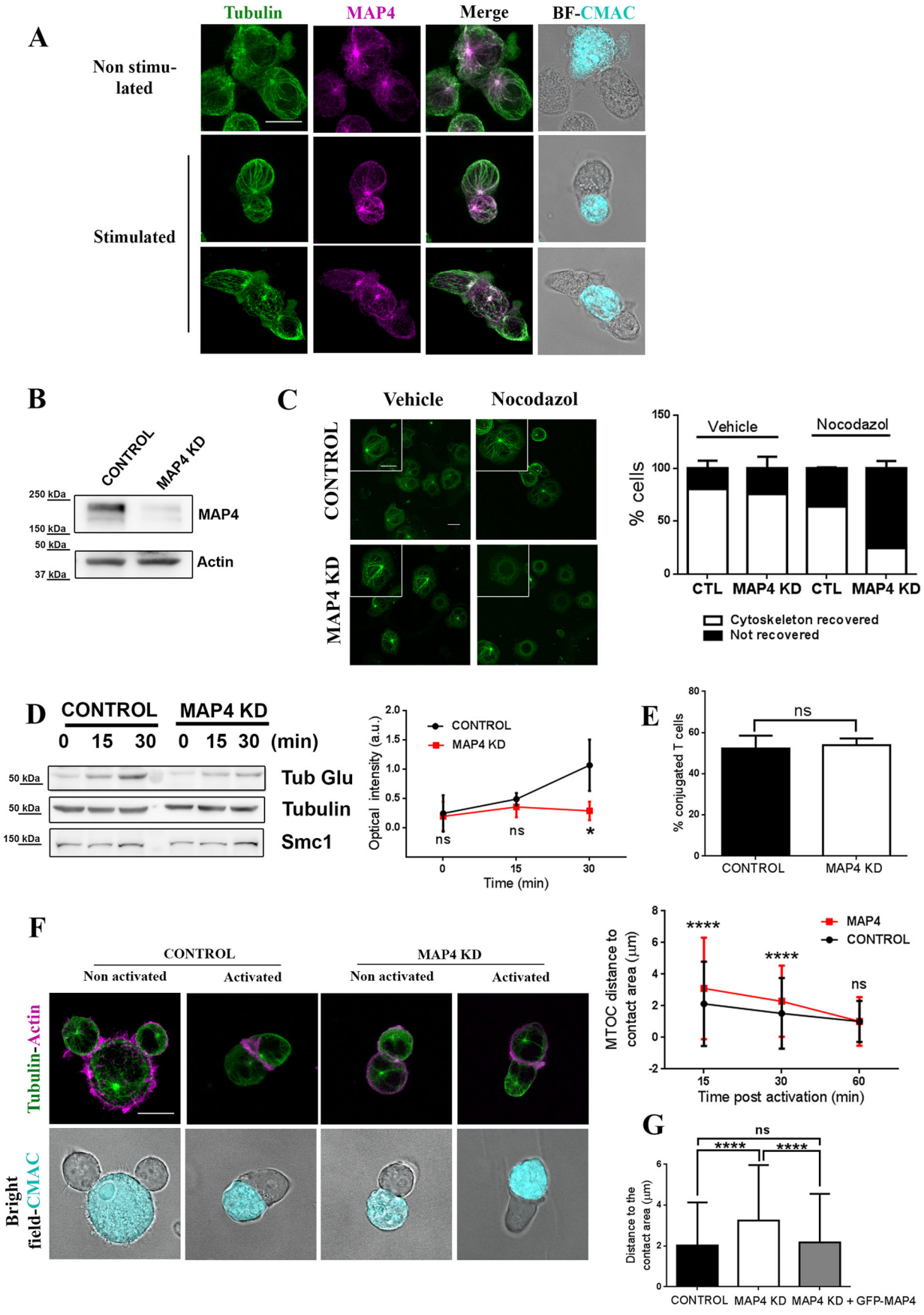

Fig. 1. See next page for legend.

Journal of Cell Science (2017) 130, 1217-1223 doi:10.1242/jcs.199042

Fig. 1. MAP4 decorates T cell MTOC and allows microtubular stability. (A) Images show conjugates of Jurkat T cells and SEE-pulsed or unpulsed Raji B cells (APCs) after 30 min. Green, α-tubulin; magenta, MAP4. A bright-field image with the cell tracker CMAC in cyan (APCs) is also shown. (B) MAP4 expression in scramble-transfected (control) and MAP4-silenced Jurkat T cells (MAP4KD). Actin is shown as a loading control. (C) Left panel, images show the recovery of MTs in MAP4KD cells treated with vehicle (DMSO) or Nocodazol (8 µM), and washed and allowed to rest for 1.5 h. Green, α-tubulin. Maximal projections are shown. The inset shows a magnification of the cells. Right panel, quantification of percentage of cells where MTs had recovered in experiments as in the left panel (at least 340 cells were counted from two different experiments). (D) Left panel, immunoblot of de-tyrosinated tubulin (Tub Glu) in control or MAP4KD cells. Cells were activated with SEE-APCs and analyzed after the indicated times. α-tubulin and Smc1 are loading controls. Right panel, quantification of the amount of detyrosinated tubulin (n=4). *P<0.05; ns, not significant (paired t-test). (E) Quantification of the percentage of control or MAP4KD T cells conjugated with SEE-APCs for 30 min (1138 and 1146 cells, from three different experiments). ns, not significant (Wilcoxon test). (F) Left panel, images show MTOC translocation in control and MAP4KD cells conjugated with unpulsed or SEE-APCs (30 min). Green, α-tubulin; magenta, β-actin. Bright field images including CMAC-labeled APCs are also shown. Right panel, quantification of the distance of MTOC to the contact area (µm) from experiments as shown in the left panel for the indicated times. Control, n=216 (15 min), 196 (30 min), 95 (60 min); MAP4KD, n=231(15 min), 251 (30 min), 105 (60 min) from three different experiments. ****P<0.0001; ns, not significant (Mann–Whitney test). (G) Quantification of the distance of MTOC to the contact area (µm) in control and MAP4KD cells transfected with GFP, or MAP4KD cells reconstituted with GFP–MAP4. n=201 (control), 216 (MAP4KD), 165 (MAP4KD+GFP–MAP4) from two independent experiments. ****P<0.0001; ns, not significant (Kruskal–Wallis test). All graphs represent mean±s.d. Scale bars: 10 µm.

The MTOC at the IS supports the generation of a new MT network near the IS, sustaining T cell signaling (Martín-Cófreces et al., 2012) and favoring the polarized secretion of vesicles to the interface between the T cell and the APC (Huse et al., 2008). Other MAPs, like HDAC6 or dynactin, are also involved in MTOC polarization. While depletion of the dynein–dynactin complex impaired the translocation of the MTOC (Martín-Cófreces et al., 2008), HDAC6 inhibition seems mostly to accelerate it either in CD4+ (Serrador et al., 2004) or CD8+ T cells (Núñez-Andrade et al., 2016). Similarly, cells depleted for the Par1b (also known as MARK2) kinase showed a defect in MTOC translocation (Lin et al., 2009). Owing to the role of MARK proteins in regulating the ability of MAP4 to bind MTs in other systems (Cheng et al., 2010), Par1b could have a role on the MAP4 effect over T cell MTs.

MAP4 modulates TCR signaling and dynamics of signaling nanovesicles at the IS

To ascertain whether the defects in the tubulin cytoskeleton seen upon MAP4 knockdown can lead to impaired signaling at the T cell receptor (TCR signalosomes), we studied the pattern of phosphorylation of downstream molecules of the TCR, such as CD3ζ, LAT, PKCθ, and ERK1 and ERK2 (ERK1/2, also known as MPAK3 and MAPK1, respectively), in SEE-activated control and MAP4KD Jurkat T cells (Fig. 2A). Quantitative analysis revealed a decrease in CD3ζ, LAT-Y191 and ERK1/2 phosphorylation and a slight decrease in LAT-Y132 phosphorylation in MAP4KD cells (Fig. 2B; Fig. S2). However, no changes in PKCθ phosphorylation were detected (Fig. S2). Likewise, CD3ζ phosphorylation in response to stimulation with anti-CD3 and anti-CD28 antibodies was impaired in MAP4KD cells (Fig. 2C,D). This reduction in CD3ζ phosphorylation may account, in part, for the defective MTOC polarization, as previously reported (Jenkins et al., 2009).

To assess the mechanism by which MAP4 regulates TCR early signaling, the dynamics of CD3ζ-bearing nanovesicles was analyzed by total internal reflection microscopy (TIRFm) in control and MAP4KD Jurkat T cells transfected with CD3ζ–Cherry and activated by a stimulatory surface coated with anti-CD3 and -CD28 antibodies. The analysis of the vesicle tracks showed a significant defect in the movement and displacement of the vesicles (Fig. 2E; Movies 2, 3). Surface levels analysis of the TCR composed of the α and β chains (encoded by *TRA* and *TRB*, respectively) and CD3ε in MAP4KD cells showed no differences (Fig. 2F). The sustained TCR signal is highly dependent on its cycle of degradation and recycling (Monjas et al., 2004). However, no differences were detected either in terms of the internalization of TCR–CD3ε molecules or in their general recycling in control and MAP4KD cells upon activation (Fig. 2G). Our results suggest that the impairment in early TCR signaling is more likely due to defects in the polarized action of CD3ζ-bearing nanovesicles rather than differences in the whole rate of internalization/recycling of the TCR. Moreover, it has been proved that a pool of active phosphorylated CD3ζ exists in the vesicular compartment that is crucial for sustaining TCR signaling and proper T cell activation (Yudushkin and Vale, 2010). Accordingly, although MAP4 reduction would probably not affect the initial triggering of TCR signaling, it leads to a blockade of the movement of the CD3ζ-containing (possibly phosphorylated) nanovesicle pool, avoiding its mobilization towards the fusion areas and therefore the maintenance of TCR signaling. On the other hand, since TCR-microcluster transport is also dependent on MTs (Hashimoto-Tane et al., 2011), we cannot rule out an additional defect on TCR-microcluster aggregation.

MAP4 absence enhances late activation markers and promotes diacylglycerol imbalance

To determine whether inhibition of TCR signaling by MAP4 depletion affects TCR-dependent gene expression or cytokine secretion, we assessed the mRNA pattern of expression of later activation markers in control or MAP4KD Jurkat T cells activated with SEE-APCs. A significant increase in IL2 and CD69 mRNA expression was detected in MAP4KD cells (Fig. 3A). Correspondingly, similar results were obtained when analyzing IL2-secretion in activated Jurkat T cells or primary T lymphoblasts (Fig. 3B). The same trend was detected when analyzing CD69 surface expression in activated Jurkat T cells (Fig. 3C) and in primary T lymphoblasts (Fig. S3A).

To explain this increase of late activation markers, we explored additional signaling intermediates downstream of the TCR. A significant increase in PLCγ1 phosphorylation in MAP4KD cells was observed both in Jurkat T cells (Fig. 3D) and in primary T lymphoblasts (Fig. 3E). To functionally analyze its relevance, we examined the production of diacylglycerol (DAG) by using the marker PKCθ-C1–GFP (containing the C1 domain of PKCθ). Quantitative analysis of its accumulation at the IS revealed a significant increase in the DAG production in MAP4KD cells (Fig. 3F). PKCθ whole protein accumulation was unaffected in MAP4KD cells (Fig. S3B). Since MAP4KD cells activated by SEE-APCs showed an increase in nuclear factor of activated T cells (NFAT) and nuclear factor κB (NF-κB) transcriptional activity (Fig. 3G), as well as in nuclear NF-κB (the p65 subunit, also known as RELA) upon TCR activation (Fig. S3C), it is possible that PKCθ is more active because of a CD28-mediated increased turnover between its plasma membrane and cytoskeleton moieties (Huang et al., 2002).

Although PLCγ1 clustering depends on LAT, PLCγ1 phosphorylation occurs prior to LAT-Y132 phosphorylation (Houtman et al., 2005) and it is dependent on Itk (Andreotti et al., 2010). In fact, our results show no differences in PLCγ1 clustering in MAP4KD cells (Fig. S3D). Therefore, MAP4 might be

Journal of Cell Science (2017) 130, 1217-1223 doi:10.1242/jcs.199042

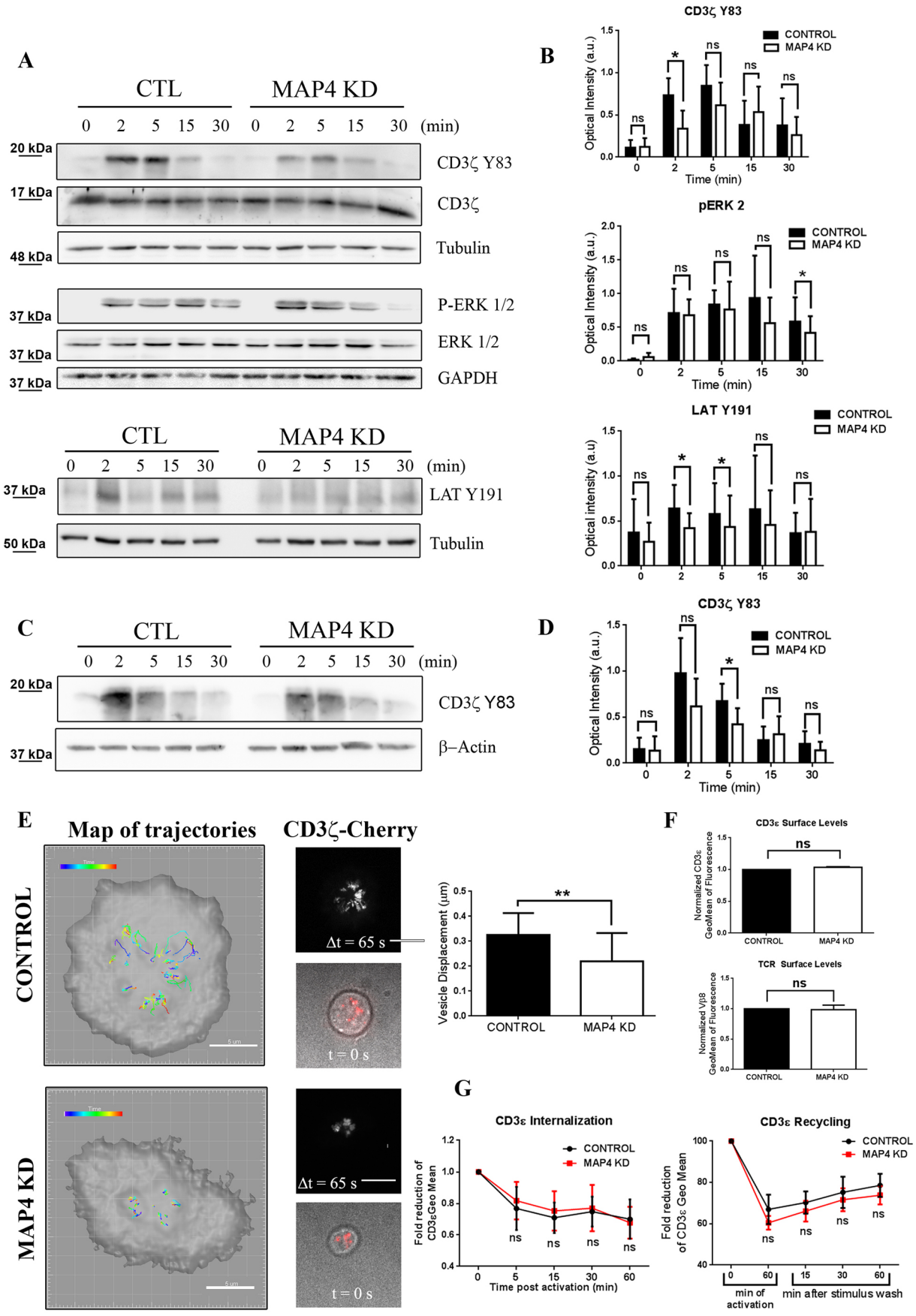

Fig. 2. See next page for legend.

Fig. 2. MAP4 sustains early T cell signaling. (A) Immunoblots showing phosphorylation of the indicated molecules (CD3ζ Y83, P-ERK1/2 and LAT Y191) in control or MAP4KD Jurkat T cells activated with SEE-pulsed Raji B cells (SEE-APCs) for the indicated times. α-tubulin, GAPDH and β-actin are loading controls. (B) Quantification (a.u., arbitrary units) of CD3ζ, ERK2 and LAT phosphorylation from experiments as in A (n=6, 7 and 6 for CD3ζ Y83, P-ERK1/2 and LAT Y191, respectively). *P<0.05; ns, not significant (paired t-test). (C) Immunoblot of CD3ζ phosphorylation (CD3ζ Y83) in control or MAP4KD cells activated with crosslinked anti-CD3 and -CD28 antibodies for the indicated times. β-actin, loading control. (D) Quantification of CD3ζ phosphorylation from experiments as in C (n=6). *P<0.05; ns, not significant (paired t-test). (E) Left panel, map of trajectories of CD3ζ–mCherry-bearing vesicles in control and MAP4KD cells spreading over anti-CD3 and -CD28-coated glass-bottom chambers. A maximal projection of a time-lapse (Δt=65 s) and initial bright field image (t=0) are shown. Right panel, quantification of the displacement length (μm) from experiments as in E (n=16 and 17 for control and MAPKD, respectively). **P<0.01 (Student's t-test). (F) Quantification by FACS of the surface basal levels of TCR (Vβ8) and CD3ε in control and MAP4KD Jurkat T cells (n=3). ns, not significant (paired t-test). (G) Quantification of CD3ε internalization (left panel) and recycling (right panel) by FACS of control or MAP4KD cells activated with anti-CD3/CD28-coated plates (n=5). ns, not significant [paired t-test (G); Wilcoxon test (F)]. All graphs represent mean±s.d.

regulating PLCγ1–Itk spatial association. Alternatively, the spatial regulation of CD148, the phosphatase responsible for PLCγ1 inactivation (Baker et al., 2001), could also be affected. Strikingly, ERK1/2 phosphorylation was reduced in MAP4KD cells. This can be explained by the defect in LAT-Y191 phosphorylation leading to a decrease in Sos–Grb2 complex recruitment and Ras pathway activation (Balagopalan et al., 2010).

In addition, local production of DAG by phosphorylated PLCγ1 (phosphorylated at Y783) can control MTOC localization close to the plasma membrane upon TCR activation (Quann et al., 2009). Our data suggest that the delay in MTOC translocation boosts the production of DAG to overcome this defect in MAP4KD cells. In accordance, preventing MTOC translocation by disruption of AKAP450 (also known as AKAP9) centrosomal localization or overexpression of HDAC6, also increased DAG production (Fig. S4). Therefore, MAP4 acts as a balancer for T cell activation and its final functional outcome.

MATERIALS AND METHODS

Cells

The human Jurkat-derived T cell line E6.1 (Vβ8$^+$ TCR) and the lymphoblastoid B-cell line Raji were from the American Type Culture Collection (ATCC). Human Cell lines were tested for mycoplasm contamination and authenticated through specific surface markers. Human peripheral blood mononuclear cells (PBMCs) were isolated from buffy coats obtained from healthy donors as described previously (Mittelbrunn et al., 2011). These studies were performed according to the principles of the Declaration of Helsinki and approved by the local Ethics Committee for

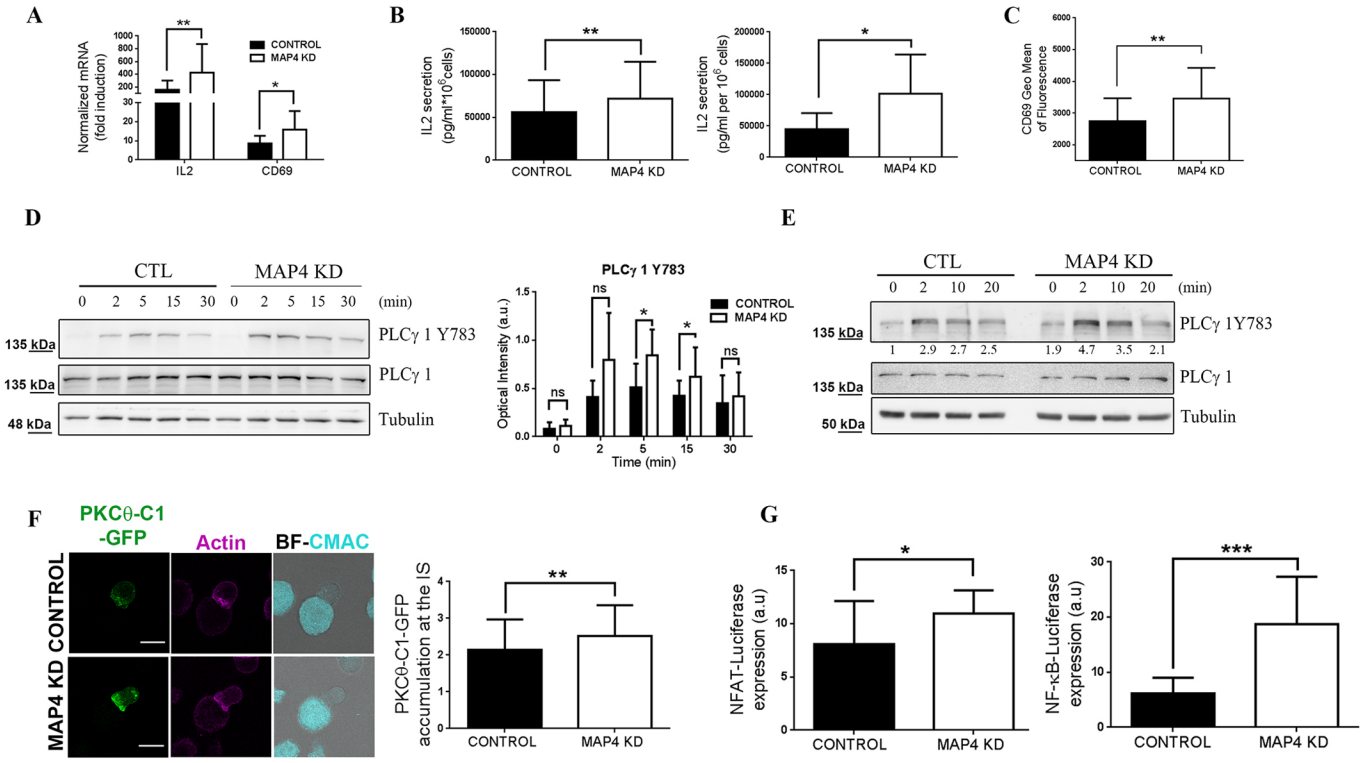

Fig. 3. MAP4 modulates DAG production and late activation markers expression. (A) mRNA levels of *IL2* and *CD69* (n=8 and 6) from control and MAP4KD cells activated with SEE-pulsed APCs (4 h). mRNA levels were normalized to a housekeeping gene (*ACTB*/*GAPDH*) and to the non-stimulated cells. *P<0.05; **P<0.01 (Wilcoxon test). (B) IL2 secretion levels (pg per ml and 10^6 cells) measured by ELISA in control and MAP4KD Jurkat T cells activated with SEE-APCs (left panel; n=7) or primaryT lymphoblasts activated with anti-CD3 and -CD28-coated plates (right panel; n=4) for 24 h. *P<0.05; **P<0.01 (paired t-test). (C) CD69 surface expression in control and MAP4KD cells activated with SEE-pulsed APCs (24 h) (n=6). **P<0.01 (paired t-test). (D) Left panel, immunoblot showing PLCγ1 phosphorylation in control and MAP4KD cells conjugated with SEE-APCs. Tubulin is shown as a loading control. Right panel, quantification of PLCγ1 phosphorylation for experiments as shown in the left panel (n=6). *P<0.05; ns, not significant (paired t-test). (E) Immunoblot showing PLCγ1 phosphorylation (PLCγ1 Y873) in control and MAP4KD primary T lymphoblasts activated with crosslinked anti-CD3 and -CD28 antibodies. Tubulin is shown as a loading control, with the quantification under bands (one representative gel out of three). (F) Left panel, images show conjugates of control and MAP4KD Jurkat T cells expressing PKCθ-C1–GFP and activated with SEE-APCs (15 min). Actin (magenta) and bright-field image with CMAC in cyan (APCs) are shown. Scale bar: 10 μm. Right panel, quantification of PKCθ-C1–GFP accumulation for experiments as in the left panel is shown (n=63 and 75 from three independent experiments). **P<0.01 (Mann–Whitney test). (G) Quantification of NFAT (left panel) and NF-κB (right panel) activity as assessed with a luciferase assay (n=6 and 5, respectively). *P<0.05; ***P<0.001 (paired t-test). All graphs represent mean±s.d.

Basic Research at the Hospital La Princesa (Madrid); informed consent was obtained from all human volunteers.

Antibodies and reagents

Antibodies used in this study were: anti-CD3ζ-pY83 (ab68236; 1:1000), anti-CD3ζ (ab190728 1:1000), anti-MAP4 [ab89650;1:800 western blotting (WB), 1:200 immunofluorescence (IF)]; anti-LAT-pY132 (ab4476 1:1000); anti-LAT-pY191 (ab59197 1:1000) (all Abcam); FITC-conjugated anti-α-tubulin (F2168; 1:100), anti-α-tubulin (T6199; 1:2000 WB), anti-β-actin (A2228; 1:1000) (all Sigma); anti-PKCθ (610090; 1:1000), anti-CD4 V450 (560346; 1:100 FACS), anti-CD3ε V500 (561416; 1:100), FITC-conjugated anti-Vβ8 (catalog number: 555606), 1:100), anti-human CD28 (555725, 3 µg/ml) (all BD-Pharmingen); anti-ERK1/2-pT202/Y204 (44285; Calbiochem; 1:1000); anti-p65 (sc372; 1:1000) (all Santa Cruz Biotechnology); anti-PKCθ-pT538 (9377 S; 1:1000), anti-PLCγ1 (2822S; 1:1000), anti-PLCγ1-pY783 (#2821L; 1:1000), anti-ERK1/2 (91075; 1:1000) (all Cell Signaling); anti-SMC1 (A300-055, 1:100) (Bethyl); anti-human CD3ε (300314, 5 µg/ml) and anti-GAPDH (649202,1:1000) (both Biolegend); Percp-Cy5.5-conjugated anti-CD19 (65-0199; 1:100); GHOST Dye Violet 510 (13-0870; 1:500 FACS) (TONBO Biosciences); FITC-conjugated anti-CD69 (21620693; 1:100) (ImmunoTools), and anti-detyrosinated tubulin (Tub Glu; Andrés-Delgado et al., 2012). Enterotoxin E (SEE) was from *Staphylococcus aureus* (Toxin Technologies). Cell tracker 7-amino-4-chloromethylcoumarin (CMAC), Prolong Gold, phalloidin and highly cross-absorbed fluorochrome-conjugated secondary antibodies were from Invitrogen. The Dual Luciferase Reporter Assay System (E1910) was from Promega. Fibronectin and poly-L-lysine were from Sigma. Horseradish peroxidase (HRP)-conjugated secondary antibodies were from Thermofisher Scientific.

Plasmids, transfection and qPCR

Plasmids encoding mouse GFP–MAP4 (Olson et al., 1995), tubulin–mCherry (Vinopal et al., 2012), the PKCθ C1 domain fused to GFP or mCherry (Carrasco and Merida, 2004), CD3ζ–mCherry (Martín-Cófreces et al., 2012), NFAT(9x)-Luciferase (Wilkins and Molkentin, 2004), NF-κB (5x)-Luciferase, provided by Maria J. Calzada (Service of Immunology, Department of Medicine, Universidad Autónoma de Madrid, Hospital Universitario de la Princesa, HUP-IIS, Madrid, Spain) and pRenilla-CMV (Promega, E226), C-term-AKAP450-GFP (Robles-Valero et al., 2010) and HDAC6–GFP (Serrador et al., 2004) were used. T cell lines were transfected with a pool of two specific double-stranded siRNAs against human MAP4 (5′-UAGGAGAGGAGAA-CCAGAU-3′ and 5′-CCAGAUUCUAUCCUCAUCU-3′) or a scramble negative control (5′-CGUACGCGGAAUACUUCGA-3′). For transfection and real-time quantitative PCR (qPCR), we followed protocols as described previously (Blas-Rus et al., 2016). Primer sequences are given in Table S1.

T cell activation, cell lysis, nuclear and cytoplasmic fractioning, and immunoblotting

For antigen stimulation, Jurkat E6.1 cells were mixed with Raji B cells (at a ratio of 1:5) pre-pulsed with 0.5 µg/ml SEE (30 min) and allowed to conjugate for the indicated times. Then, cells were lysed and immunoblotting was performed as described previously (Blas-Rus et al., 2016). For nuclear–cytoplasmic fractioning, cells were lysed and spun at 650 ***g*** (15 min/4°C), and supernatant was recovered as the cytoplasmic fraction. The pellet was washed once with lysis buffer without NP-40 and lysed in loading buffer and taken as the nuclear fraction.

Cell conjugate formation, immunofluorescence and TIRFm

Cell conjugation preparation, immunoflorescence protocols, confocal and TIRFm imaging were performed as described previously (Blas-Rus et al., 2016). Specific conditions are described in corresponding figure legends. For MAP4 staining, cells were fixed in 100% methanol (5 min at −20°C) followed by 2% paraformaldehyde (10 min at room temperature). Images were processed, and quantified with Adobe Photoshop CS and ImageJ. MTOC translocation experiment images were analyzed with Imaris software.

Nocodazol treatment

Cells were treated with vehicle (DMSO) or nocodazol (8 µM) for 1 h, washed twice and left to recover for 1.5 h.

ELISA, flow cytometry and TCR internalization and recycling measurement

Jurkat E6.1T cells were co-cultured with SEE-pulsed Raji B cells (at a ratio of 1:1) for 24 h. For primary T cell lymphocytes, cells were stimulated with anti-CD3 and anti-CD28 antibody-coated plates. Cells were used for flow cytometry (FACS) analysis and supernatant for IL-2 detection by ELISA (DyaClone). For FACS, cells were incubated with primary and secondary antibodies (30 min at 4°C). Cells were washed and fixed in IC Fixation Buffer (eBioscience) (20 min at 4°C).

For TCR internalization measurement, Jurkat E6.1 cells were stimulated with anti-CD3ε (HIT3α) and -CD28 antibody-coated plates for the indicated times. Cells were then fixed and stained for CD3ε (UCHT1). Cells were analyzed with a FACs Canto II Cytometer (BD) and FlowJo. Recycling experiments were performed as described previously (Finetti et al., 2009). Stimulation was performed with anti-CD3 and anti-CD28 antibody-coated plates.

Luciferase assay

Cells were transfected with NFAT- and NFκB-promoter-driven Luciferase constructions plus *Renilla* plasmid (2 µg+0.4 µg per 10^6 of cells, respectively) and activated with SEE-pulsed-Raji B cells (24 h). The protocol was performed accordingly to manufacturer's instructions (Promega). Measurements were normalized to *Renilla* levels and protein quantity.

Statistical analysis

Data was analyzed with a ROUT test, to detect outliers, and a Shapiro–Wilk normality test to determine the application of parametric or non-parametric tests. A Student-*t*-test (parametric) or *U*-Mann–Whitney (non-parametric) analysis was used for pairs of non-dependent data. A Kruskal–Wallis test was used for grouped analysis. Finally, when compared samples were activated under the same conditions (dependent samples) a paired analysis was used; either a paired *t*-test (parametric) or Wilcoxon test (non-parametric). Analysis was performed with GraphPad Prism.

Acknowledgements

We thank Dr Miguel Vicente Manzanares for critical reading of the manuscript and Aitana Sanguino Pascual for technical support.

Competing interests

The authors declare no competing or financial interests.

Author contributions

E.B.-M. and F.S.-M. designed experiments, made figures and wrote the manuscript; E.B.-M.; N.B.-R.; N.B.M.-C. collected and/or analyzed data.

Funding

This study was supported by grants from the Ministerio de Economía y Competitividad (SAF2014-55579-R), Consejería de Educación, Juventud y Deporte (INDISNET-S2011/BMD-2332) and European Research Council (ERC-2011-AdG 294340-GENTRIS). The Centro Nacional de Investigaciones Cardiovasculares (CNIC, Spain) is supported by the Ministerio de Ciencia e Innovación and the Pro-CNIC Foundation. The Centros de Investigación Biomédica en Red (CIBER) is supported by the Instituto de Salud Carlos III and co-funding from Fondo Europeo de Desarrollo Rural (FEDER). E.B.-M. was supported by the Pro-CNIC Foundation and Obra Social La Caixa.

Supplementary information

Supplementary information available online at
http://jcs.biologists.org/lookup/doi/10.1242/jcs.199042.supplemental

References

Andreotti, A. H., Schwartzberg, P. L., Joseph, R. E. and Berg, L. J. (2010). T-cell signaling regulated by the Tec family kinase, Itk. *Cold Spring Harb. Perspect. Biol.* **2**, a002287.

Andrés-Delgado, L., Antón, O. M., Bartolini, F., Ruiz-Sáenz, A., Correas, I., Gundersen, G. G. and Alonso, M. A. (2012). INF2 promotes the formation of detyrosinated microtubules necessary for centrosome reorientation in T cells. *J. Cell Biol.* **198**, 1025-1037.

Baker, J. E., Majeti, R., Tangye, S. G. and Weiss, A. (2001). Protein tyrosine phosphatase CD148-mediated inhibition of T-cell receptor signal transduction is

associated with reduced LAT and phospholipase Cgamma1 phosphorylation. *Mol. Cell. Biol.* **21**, 2393-2403.

Balagopalan, L., Coussens, N. P., Sherman, E., Samelson, L. E. and Sommers, C. L. (2010). The LAT story: a tale of cooperativity, coordination, and choreography. *Cold Spring Harb. Perspect. Biol.* **2**, a005512.

Blas-Rus, N., Bustos-Morán, E., Pérez de Castro, I., de Cárcer, G., Borroto, A., Camafeita, E., Jorge, I., Vázquez, J., Alarcón, B., Malumbres, M. et al. (2016). Aurora A drives early signalling and vesicle dynamics during T-cell activation. *Nat. Commun.* **7**, 11389.

Carrasco, S. and Merida, I. (2004). Diacylglycerol-dependent binding recruits PKCtheta and RasGRP1 C1 domains to specific subcellular localizations in living T lymphocytes. *Mol. Biol. Cell* **15**, 2932-2942.

Chang, W., Gruber, D., Chari, S., Kitazawa, H., Hamazumi, Y., Hisanaga, S. and Bulinski, J. C. (2001). Phosphorylation of MAP4 affects microtubule properties and cell cycle progression. *J. Cell Sci.* **114**, 2879-2887.

Cheng, G., Takahashi, M., Shunmugavel, A., Wallenborn, J. G., DePaoli-Roach, A. A., Gergs, U., Neumann, J., Kuppuswamy, D., Menick, D. R. and Cooper, G. IV. (2010). Basis for MAP4 dephosphorylation-related microtubule network densification in pressure overload cardiac hypertrophy. *J. Biol. Chem.* **285**, 38125-38140.

Finetti, F., Paccani, S. R., Riparbelli, M. G., Giacomello, E., Perinetti, G., Pazour, G. J., Rosenbaum, J. L. and Baldari, C. T. (2009). Intraflagellar transport is required for polarized recycling of the TCR/CD3 complex to the immune synapse. *Nat. Cell Biol.* **11**, 1332-1339.

Ghossoub, R., Hu, Q., Failler, M., Rouyez, M.-C., Spitzbarth, B., Mostowy, S., Wolfrum, U., Saunier, S., Cossart, P., James Nelson, W. et al. (2013). Septins 2, 7 and 9 and MAP4 colocalize along the axoneme in the primary cilium and control ciliary length. *J. Cell Sci.* **126**, 2583-2594.

Hashimoto-Tane, A., Yokosuka, T., Sakata-Sogawa, K., Sakuma, M., Ishihara, C., Tokunaga, M. and Saito, T. (2011). Dynein-driven transport of T cell receptor microclusters regulates immune synapse formation and T cell activation. *Immunity* **34**, 919-931.

Houtman, J. C. D., Houghtling, R. A., Barda-Saad, M., Toda, Y. and Samelson, L. E. (2005). Early phosphorylation kinetics of proteins involved in proximal TCR-mediated signaling pathways. *J. Immunol.* **175**, 2449-2458.

Huang, J., Lo, P.-F., Zal, T., Gascoigne, N. R. J., Smith, B. A., Levin, S. D. and Grey, H. M. (2002). CD28 plays a critical role in the segregation of PKC theta within the immunologic synapse. *Proc. Natl. Acad. Sci. USA* **99**, 9369-9373.

Huppa, J. B. and Davis, M. M. (2003). T-cell-antigen recognition and the immunological synapse. *Nat. Rev. Immunol.* **3**, 973-983.

Huse, M., Quann, E. J. and Davis, M. M. (2008). Shouts, whispers and the kiss of death: directional secretion in T cells. *Nat. Immunol.* **9**, 1105-1111.

Jenkins, M. R., Tsun, A., Stinchcombe, J. C. and Griffiths, G. M. (2009). The strength of T cell receptor signal controls the polarization of cytotoxic machinery to the immunological synapse. *Immunity* **31**, 621-631.

Lin, J., Hou, K. K., Piwnica-Worms, H. and Shaw, A. S. (2009). The polarity protein Par1b/EMK/MARK2 regulates T cell receptor-induced microtubule-organizing center polarization. *J. Immunol.* **183**, 1215-1221.

Martín-Cófreces, N. B., Robles-Valero, J., Cabrero, J. R., Mittelbrunn, M., Gordón-Alonso, M., Sung, C.-H., Alarcón, B., Vázquez, J. and Sánchez-Madrid, F. (2008). MTOC translocation modulates IS formation and controls sustained T cell signaling. *J. Cell Biol.* **182**, 951-962.

Martín-Cófreces, N. B., Baixauli, F., López, M. J., Gil, D., Monjas, A., Alarcón, B. and Sánchez-Madrid, F. (2012). End-binding protein 1 controls signal propagation from the T cell receptor. *EMBO J.* **31**, 4140-4152.

Martín-Cófreces, N. B., Baixauli, F. and Sánchez-Madrid, F. (2014). Immune synapse: conductor of orchestrated organelle movement. *Trends Cell Biol.* **24**, 61-72.

Mittelbrunn, M., Gutiérrez-Vázquez, C., Villarroya-Beltri, C., González, S., Sánchez-Cabo, F., González, M. A., Bernad, A. and Sánchez-Madrid, F. (2011). Unidirectional transfer of microRNA-loaded exosomes from T cells to antigen-presenting cells. *Nat. Commun.* **2**, 282.

Mogessie, B., Roth, D., Rahil, Z. and Straube, A. (2015). A novel isoform of MAP4 organises the paraxial microtubule array required for muscle cell differentiation. *Elife* **4**, e05697.

Monjas, A., Alcover, A. and Alarcon, B. (2004). Engaged and bystander T cell receptors are down-modulated by different endocytotic pathways. *J. Biol. Chem.* **279**, 55376-55384.

Nguyen, H. L., Gruber, D., McGraw, T., Sheetz, M. P. and Bulinski, J. C. (1998). Stabilization and functional modulation of microtubules by microtubule-associated protein 4. *Biol. Bull.* **194**, 354-357.

Nguyen, H. L., Gruber, D. and Bulinski, J. C. (1999). Microtubule-associated protein 4 (MAP4) regulates assembly, protomer-polymer partitioning and synthesis of tubulin in cultured cells. *J. Cell Sci.* **112**, 1813-1824.

Núñez-Andrade, N., Iborra, S., Trullo, A., Moreno-Gonzalo, O., Calvo, E., Catalán, E., Menasche, G., Sancho, D., Vázquez, J., Yao, T.-P. et al. (2016). HDAC6 regulates the dynamics of lytic granules in cytotoxic T lymphocytes. *J. Cell Sci.* **129**, 1305-1311.

Olson, K. R., McIntosh, J. R. and Olmsted, J. B. (1995). Analysis of MAP 4 function in living cells using green fluorescent protein (GFP) chimeras. *J. Cell Biol.* **130**, 639-650.

Quann, E. J., Merino, E., Furuta, T. and Huse, M. (2009). Localized diacylglycerol drives the polarization of the microtubule-organizing center in T cells. *Nat. Immunol.* **10**, 627-635.

Robles-Valero, J., Martin-Cofreces, N. B., Lamana, A., Macdonald, S., Volkov, Y. and Sanchez-Madrid, F. (2010). Integrin and CD3/TCR activation are regulated by the scaffold protein AKAP450. *Blood* **115**, 4174-4184.

Samora, C. P., Mogessie, B., Conway, L., Ross, J. L., Straube, A. and McAinsh, A. D. (2011). MAP4 and CLASP1 operate as a safety mechanism to maintain a stable spindle position in mitosis. *Nat. Cell Biol.* **13**, 1040-1050.

Serrador, J. M., Cabrero, J. R., Sancho, D., Mittelbrunn, M., Urzainqui, A. and Sánchez-Madrid, F. (2004). HDAC6 deacetylase activity links the tubulin cytoskeleton with immune synapse organization. *Immunity* **20**, 417-428.

Soares, H., Lasserre, R. and Alcover, A. (2013). Orchestrating cytoskeleton and intracellular vesicle traffic to build functional immunological synapses. *Immunol. Rev.* **256**, 118-132.

Vinopal, S., Černohorská, M., Sulimenko, V., Sulimenko, T., Vosecká, V., Flemr, M., Dráberová, E. and Dráber, P. (2012). gamma-Tubulin 2 nucleates microtubules and is downregulated in mouse early embryogenesis. *PLoS ONE* **7**, e29919.

Wilkins, B. J. and Molkentin, J. D. (2004). Calcium-calcineurin signaling in the regulation of cardiac hypertrophy. *Biochem. Biophys. Res. Commun.* **322**, 1178-1191.

Yudushkin, I. A. and Vale, R. D. (2010). Imaging T-cell receptor activation reveals accumulation of tyrosine-phosphorylated CD3zeta in the endosomal compartment. *Proc. Natl. Acad. Sci. USA* **107**, 22128-22133.